



Trade Science Inc.

ISSN : 0974 - 7443

Volume 7 Issue 2

**CHEMICAL TECHNOLOGY**

*An Indian Journal*

*Full Paper*

CTAIJ 7(2) 2012 [45-51]

## Solution route synthesis of selenium (IV)-doped- $\text{LiMn}_{2-x}\text{Se}_x\text{O}_4$ spinel for promoting structural and microstructural features of lithium ion batteries

Khaled M.Elsabawy\*<sup>1,2</sup>

<sup>1</sup>Materials Science Unit, Chemistry Department, Faculty of Science, 31725, Tanta University, (EGYPT)

<sup>2</sup>Materials Science Unit, Chemistry Department, Faculty of Science, Taif University, Alhawayah, 888, (SAUDIARABIA)

E-mail: ksabawy@yahoo.com

Received: 5<sup>th</sup> May, 2012 ; Accepted: 30<sup>th</sup> July, 2012

### ABSTRACT

The spinel structure with chemical formula  $\text{LiMn}_2\text{O}_4$  and doped samples with the general formula  $\text{LiMn}_{2-x}\text{Se}_x\text{O}_4$ , where  $x = 0.02, 0.04$  mole were prepared by freeze dry technique and sintering procedure using the appropriate amounts of nitrate solutions precursors. The structural, microstructural and electrochemical features of pure spinel and Se-(IV)-doped samples were investigated. XRD-analysis indicated that all of the prepared samples are mainly belong to cubic crystal form with Fd3m space group. Electrochemical investigations indicated that selenium doping promotes both of the retention capacity a recharging efficiency.

© 2011 Trade Science Inc. - INDIA

### KEYWORDS

Li-ion batteries;  
Selenium-doping;  
Crystal structure;  
SEM;  
XRD.

### INTRODUCTION

The lithium ion batteries are consisting of lithium intercalation compounds as positive electrode, graphite or carbon as negative electrode, and an organic electrolyte are under consideration for the electric vehicle and the hybrid electric vehicle applications. The technological challenges confronting their scale up and commercialization are the capacity fade characteristics and the thermal safety. The cathode materials such as  $\text{LiCoO}_2$  [1,2],  $\text{LiNiO}_2$  [3,4],  $\text{LiNi}_y\text{Co}_{1-y}\text{O}_2$  [5,6] are currently used in the lithium-ion batteries. Although the commercially available lithium-ion cells for portable applications use  $\text{LiCoO}_2$  and  $\text{LiCo}_y\text{Ni}_{1-y}\text{O}$ , they are considered to be more expensive and toxic than that having a  $\text{LiMn}_2\text{O}_4$  cathode. The  $\text{LiMn}_2\text{O}_4$  has been studied extensively as a cathode material for Li-ion batteries because it is relatively inexpensive and has environmental

advantages, compared with  $\text{LiCoO}_2$ ,  $\text{LiNiO}_2$ , and  $\text{LiNi}_y\text{Co}_{1-y}\text{O}_2$  [1-6]. However,  $\text{LiMn}_2\text{O}_4$  shows problems related to poor cycling behavior because of a fast capacity fading in the three voltage range due to the phase transformation from cubic structure to tetragonal structure and also in the four voltage range mainly due to the Mn ( $\text{Mn}^{3+}$ ) dissolution during lithium ion intercalation/deintercalation [7]. Reducing the amount of the  $\text{Mn}^{3+}$  ion in structure may help in improving the cycling performance of Mn spinel [8-10]. Transitional metals in the same row in the periodic table may be considered as the possible candidates for the substitution because of their similar ionic radii. The use of metal ions with similar radii will not cause a dramatic structural change as a result of the substitution [11-15]. In an effort to better understand the performance issues of the Mn spinels, research was undertaken to prepare the manganese-substituted spinels by partially substituting Mn separately with Co,

## Full Paper

Ni, Fe and Cr studying their structures, electrochemical behavior, diffusion phenomena and thermal characteristics. A sol-gel process was used for the synthesis in order to achieve the homogeneity and narrow particle size distribution of the final product<sup>[16-19]</sup>. The electrochemical and thermal properties of the substituted LiMn<sub>2</sub>O<sub>4</sub> spinels were compared with those of LiMn<sub>2</sub>O<sub>4</sub>.

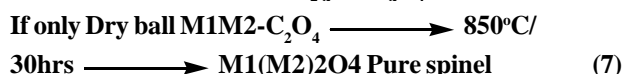
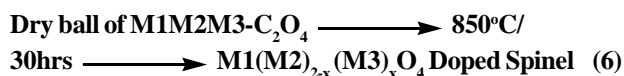
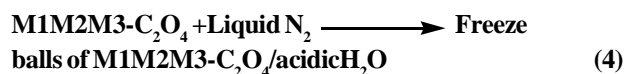
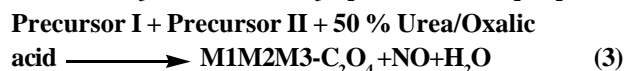
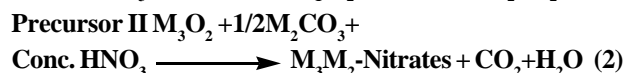
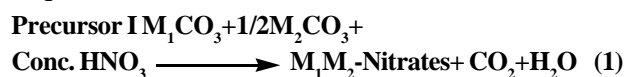
The major goal of the present article is to investigate narrow range of Se (IV) ions doping on manganese sites (0.02 d'' x d'' 0.04) To promote:

- 1- Structural and micro-structural features of cubic spinel (Li-Mn-O).
- 2- Cathodic features (specially charge/discharge specific capacity and cycleability).

### EXPERIMENTAL

#### Freeze dry synthesis of Li-Mn-O spinels

The pure spinel LiMn<sub>2</sub>O<sub>4</sub> and doped samples with the general formula LiMn<sub>2-x</sub>Se<sub>x</sub>O<sub>4</sub>, where x = 0.02, 0.04 mole were prepared by freeze dry technique and sintering procedure using the appropriate amounts of nitrate solutions precursors. The precursor (I) was the accurate molar ratios of Li<sub>2</sub>CO<sub>3</sub> and 1<sup>st</sup> half of Mn<sub>2</sub>(CO<sub>3</sub>)<sub>3</sub> weight that dissolved in few drops of conc. nitric acid giving metal nitrates solutions. The precursor II was for SeO<sub>2</sub> and 2<sup>nd</sup> half of Mn<sub>2</sub>(CO<sub>3</sub>)<sub>3</sub> (each purity >99%) that also dissolved in few drops of conc. nitric acid giving metal nitrates solutions. The precursors I + II were mixed together into 1L separating funnel contain 100 ml of 50 % solution of urea/ oxalic acid then allow to drop into liquid nitrogen getting freeze drops of mixtures. Generally the synthesis of pure spinel and selenium doped spinels can be briefed in the following sequences;



Where M<sub>1</sub> = Li, M<sub>2</sub> = Mn (III) and finally M<sub>3</sub> = Se (IV).

The resulted freeze drops forwarded to freeze dry machine with specific program of acidic water solvent for 60 hrs. The resultant reground in an agate mortar for half an hour. Then the finely ground powder was subject to firing at 800 °C for 10 hours, reground and finally pressed into pellets with thickness 0.2 cm, diameter 1.2 cm and Sintered at 850 °C for 30 hours. Then the furnace is cooled slowly down to room temperature. Finally the materials are kept in vacuum desiccator over silica gel dryer.

#### Structural characterization

##### X-ray diffraction (XRD)

The X-ray diffraction measurements (XRD) were carried out at room temperature on the fine ground pure and Se-substituted spinels in the range (2θ = 10-90°) using Cu-Kα radiation source and a computerized [Steo-Germany] X-ray diffractometer with two theta scan technique. A visualized studies of crystal structure were made by using Diamond Molecular Structure version 3.2 package, Germany.

##### Scanning electron-microscope

Scanning electron microscope (SEM) measurements were carried out using small pieces of prepared samples on different sectors to be the actual molar ratios by using "TXA-840, JEOL-Japan" attached to XL30 apparatus with EDX unit, accelerant voltage 30kv, magnification 10x up to 500.000x and resolution 3. nm. The samples were coated with gold.

##### Electrochemical measurements

The coin cells model (2016 size) were used for electrochemical. The coin cells comprised of LiMn<sub>2-x</sub>Se<sub>x</sub>O<sub>4</sub> as a cathode, lithium foil anode, and an electrolyte having 0.5 M LiPF<sub>6</sub> in a 1:1 wt.% of ethylene carbonate and diethyl carbonate (EC/DEC, EM Industry, Inc. H<sub>2</sub>O < 30 ppm). A Celgard 2400 micro-porous polypropylene separator was used in these cells. The cell preparation was carried out in the Argon-filled dry box. The cells were first cycled three times and then, charged to

4.5 V. The cells were charged using a constant voltage charging procedure for 40 h. The cut-off voltage for charging was 4.5 V. The charged coin cells were opened in an argon-filled glove box and the cathode material was recovered from the cells.

## RESULTS AND DISCUSSION

### Phase identification

Figure 1<sub>a-c</sub> shows the X-ray diffraction patterns of pure spinel and Se-doped spinels with formula  $\text{LiMn}_{2-x}\text{Se}_x\text{O}_4$  (where  $x=0.02, 0.04$  mole) powders. Analysis of the corresponding  $2\theta$  values and the interplanar spacings  $d$  ( $\text{\AA}$ ) indicated that the compounds are mainly belong to a single-phase spinel structure, with  $Fd3m$  space group in which the lithium ions occupy the tetrahedral ( $9_a$ ) sites as clear in Figure 1<sub>d</sub>. The  $\text{Mn}^{3+}$  and

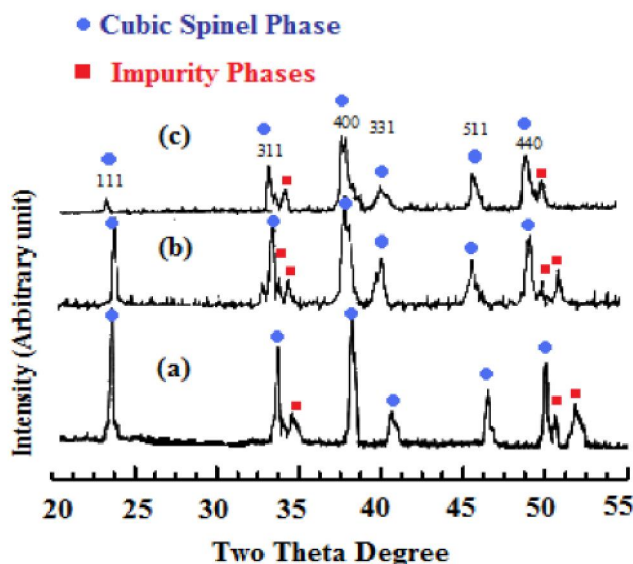


Figure 1<sub>a-c</sub>: X-ray diffraction patterns of  $\text{LiMn}_{2-x}\text{Se}_x\text{O}_4$  spinel doped with  $\text{Se}^{4+}$ . (a): undoped  $\text{LiMn}_2\text{O}_4$ ; (b): doped with  $x = 0.02$  mole; (c): doped with  $x = 0.04$  mole.

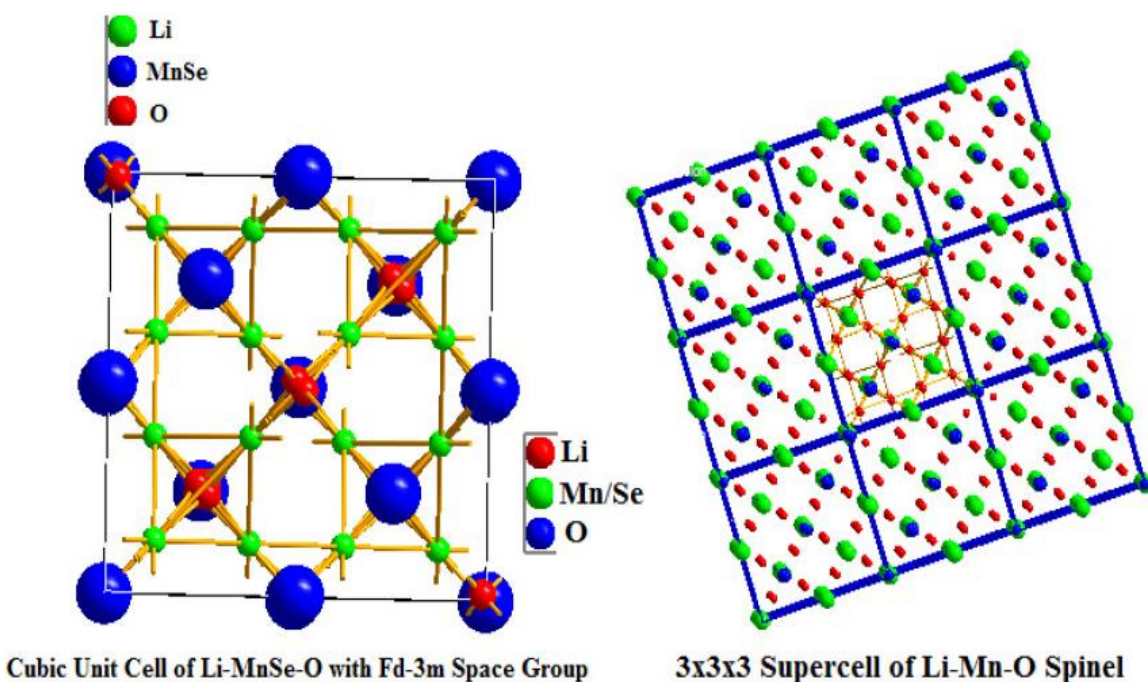


Figure 1<sub>d</sub>: Visualized structure of cubic spinel with  $Fd3m$  space group.

$\text{Mn}^{4+}$  ions as well as the doping metal ions, as in  $\text{LiMn}_2\text{O}_4$  structure, occupy the octahedral ( $16_d$ ) sites<sup>[19]</sup>. For simplicity, these structures can be expressed as  $[\text{Li}]^{\text{tetrahedral}}[\text{M}_y\text{Mn}_{2-y}]^{\text{octahedral}}[\text{O}_4]^{\text{[20]}}$  as described in figure 1d. Doping did not appear to change the basic  $\text{LiMn}_2\text{O}_4$  structure, but slightly change the lattice parameters due to atom size effect.

As clear in Figures 1<sub>a-d</sub> the Li-Mn-O spinel doped with  $\text{Se}^{4+}$  of at the expense of  $\text{Mn}^{3+}$  crystallized in octa-

hedral units  $[\text{MnO}_6]$  without any kind of noticeable distortion as expected with  $Fd3m$  space group. Only  $\text{Mn}^{II}$  oxide as secondary phase appears in minor trace in the background which confirm success of selenium-doping in the investigated range.

It is well known that spinel  $\text{LiMn}_2\text{O}_4$  as a cathodic material is too poor to be substituted or replaced by  $\text{LiCoO}_2$  due to the gradual degradation of its capacity on cycling. The degradation mechanisms have been pro-

## Full Paper

posed as (a) structural damage due to Jahn-Teller distortion, (b) dissolution of the spinel into the electrolyte, (c) oxidation of the electrolyte on the surface of the cathode at the highly charged state<sup>[21-25]</sup>.

Accurate retvield analysis of structure indicated that all samples have the finger print peaks of Li-Mn-O spinel (red circles in Figure 1<sub>a-c</sub>) with high degree of crystallinity.

The lattice constants of cubic spinels were calculated and found to be  $a = 8.2879(1) \text{ \AA}$  for  $x = 0.02$  mole and  $a = 8.2803(4) \text{ \AA}$  for  $x = 0.04$  mole which are lower than undoped one ( $a = 8.2896(3)$ ) since the radii of the sixth coordinate Se<sup>4+</sup> and Mn<sup>3+</sup> are 0.050 and 0.066 nm, respectively. So that the unite crystal volume compresses, that what was expected, and in

full agreement with Xu et al.<sup>[26]</sup>.

These results in full agreement with those reported by Wolska et al.<sup>[27]</sup> who stated that substitution with very small quantities of Fe<sup>+++</sup> ions first restrains the partial ordering of Mn<sup>3+</sup> and Mn<sup>4+</sup> ions in the spinel superlattice and then stabilizes cubic spinel structure of LiMn<sub>2</sub>O<sub>4</sub>.

Confirmation of synthesized pure spinel and Se-doped spinels with formula LiMn<sub>2-x</sub>Se<sub>x</sub>O<sub>4</sub> (where  $x = 0.02, 0.04$  mole) structures were performed through theoretical treatment by visualizing of structures of both experimental and theoretical lattice coordinates of spinel structure (Figure 1<sub>d,1e</sub>) via Diamond Impact Crystal package.

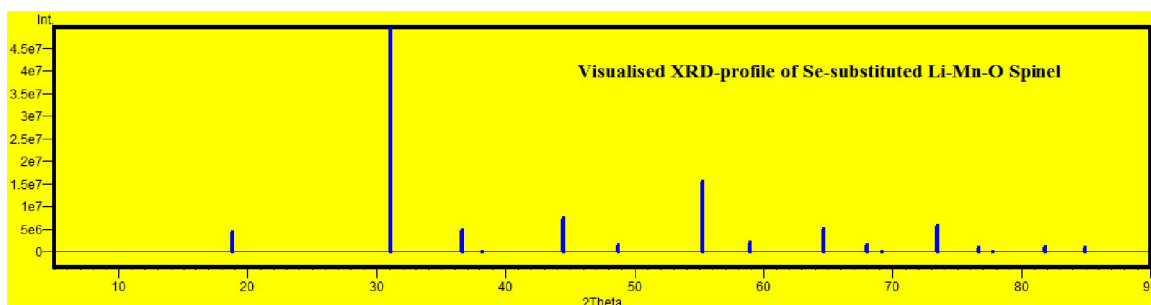


Figure 1<sub>c</sub> : Visualized XRD-profile for LiMn<sub>2</sub>O<sub>4</sub> spinel.

The study made was concerned by matching and comparison of calculated and theoretical data as bond distances, oxidation states and bond torsion on the crystal structure formed. The comparison between experimental and theoretical data exhibited moderate fitting of peak positions between experimental and theoretical data (Figure 1e) confirming that Se-IV substitutes successfully on crystal structure on Mn (III) sites in the investigation range.

The analysis of bond distances and angles recorded in TABLE 1 and 2 one can notify that there are no violation on the MnSe-O bond distances observed which reflect the narrow ratio of dopant element (Se<sup>++++</sup>) ion does not cause any kind of distortion inside polyoctahedrons and consequently lattice structure of spinel.

Furthermore the torsions on the bonds angle inside lattice and superlattice of Se-doped spinels does not destroy spinel structure which reflect suitability and fitting between doping element and substituted manganese (III) sites.

### Scanning electron microscopy

The morphology of powdered samples for undoped

and doped sample fired at 750°C in air for 50 hr, were investigated by scanning electron microscope (SEM) after coating with gold. Figure 2<sub>a-c</sub> represents the captured images for undoped LiMnO<sub>4</sub> powder and Se-doped spinels. with low – magnification of 750 times, the morphology of this powder reveals that the powder exhibits irregular porous agglomerates. It can be more clearly observed that there are many micro – holes in the surface of the particles, this porous morphology is beneficial for the diffusion of electrolyte into the interior of the particle during fabrication of the battery. The formation of porous morphology is attributed to the release of the gases such as CO<sub>2</sub> and H<sub>2</sub>O from the interior of the particles during the heat treatment. In other words, the organic constituents in LiMnC<sub>2</sub>O<sub>4</sub> (AC) precursor has bubbling effect. The morphology of the same sample (LiMn<sub>2</sub>O<sub>4</sub>) doped with Se ( $x = 0.02$  and  $x = 0.04$  mole) with magnification of 35000 times. Figure 2b,c reveal that the sample have regular nano – sized grains of average size 137 nm and the average particle size is ~ 15.6 nm.

These averages of grain and particle size of pure

and Se-doped spinels are fully consistent with those reported by Lu et al.<sup>[28]</sup> who synthesized uniform spinel by using emulsion technique with spherical powders with a size distribution which ranged from 0.1- 0.15  $\mu\text{m}$ .

### Electrochemical measurements

#### Specific capacities investigations

Figure 3<sub>A-C</sub> shows the initial and tenth charge–discharge curves of Li/LiMn<sub>2-x</sub>Se<sub>x</sub>O<sub>4</sub> coin cells where x = 0.0, 0.02 and 0.04 mole respectively at a constant charge–discharge rate of C/15 over the voltage range of 4.5–3V. The theoretical and experimental capacities are compared.

The theoretical capacity of the Li/LiMn<sub>2</sub>O<sub>4</sub> cell is 148 mA h g<sup>-1</sup><sup>[29]</sup> on the basis that one Li per Mn<sub>2</sub>O<sub>4</sub> unit is reversibly intercalated and deintercalated at 4.12 V. But, LiMn<sub>2</sub>O<sub>4</sub> shows actual value of about 125 mA h g<sup>-1</sup> corresponding to 0.81–0.89 of total Li in LiMn<sub>2</sub>O<sub>4</sub> reversibly utilized within the voltage range of 3.–4.5 V. While the specific capacities recorded for first charge and discharge curve of Se-substituted spinels were 123 and 119 mA h g<sup>-1</sup> respectively.

It was observed that for the first ten cycles the capacity retentions (loss with cycleability) were promoted as selenium doping increases recording maximum for x = 0.04 mole (0.42 % loss per cycle) and 0.48 % loss per cycle for LiMn<sub>1.95</sub>Se<sub>0.02</sub>O<sub>4</sub> and minimum one for the undoped parent LiMn<sub>2</sub>O<sub>4</sub> which equal to 1.76 %

TABLE 1 : Some selected lattice coordinates, bond distances inside unit cell of Se-substituted Spinel Li-Mn-O.

Table 1		Lattice Coordinates			Bond Distance
Atom 1	Atom 2	x/a	y/b	z/y	d Å <sup>o</sup>
Li1	O1	0.0124	0.0124	-0.0124	1.7415
Li1	O1	0.0124	-0.0124	0.0124	1.7415
Li1	O1	-0.0124	0.0124	0.0124	1.7415
Li1	O1	0.2624	0.2376	0.2376	1.7415
Li1	O1	0.2376	0.2376	0.2624	1.7415
Li1	O1	0.2376	0.2624	0.2376	1.7415
Li1	Mn1 Se1	0.2500	0.2500	0.2500	1.7927
Li1	O1	-0.0124	-0.0124	-0.0124	1.9705
Li1	O1	0.2624	0.2624	0.2624	1.9705
Mn1 Se1	O1	0.4876	-0.0124	0.4876	0.1778
Mn1 Se1	O1	0.4876	0.0124	0.5124	0.1778
Mn1 Se1	O1	0.5124	-0.0124	0.5124	0.1778
Mn1 Se1	O1	0.5124	0.0124	0.4876	0.1778
Mn1 Se1	Li1	0.3750	-0.125	0.6250	1.7927
Mn1 Se1	Li1	0.6250	-0.125	0.3750	1.7927
Mn1 Se1	Li1	0.6250	0.1250	0.6250	1.7927
Mn1 Se1	Li1	0.3750	0.1250	0.3750	1.7927
O1	Mn1 Se1	0.2500	0.2500	0.2500	0.1778
O1	O1	0.2376	0.2376	0.2624	0.2904
O1	O1	0.2624	0.2376	0.2376	0.2904
O1	O1	0.2376	0.2624	0.2376	0.2904
O1	Li1	0.3750	0.1250	0.3750	1.7415
O1	Li1	0.3750	0.3750	0.1250	1.7415
O1	Li1	0.1250	0.3750	0.3750	1.7415

TABLE 2 : Some selected symmetry operations and angles inside unit cell of Se-substituted spinel Li-Mn-O.

Atom1	Atom2	Symmetry Op.1	Atom3	Symmetry Op.2	Angle213
	O1	0.25-y, -0.25+x, -0.25+z	O1	-0.25+x, -0.25+z, 0.25-y	9.565
	O1	0.25-y, -0.25+x, -0.25+z	O1	x, 0.5-y, 0.5-z	180.000
	O1	0.25-y, -0.25+x, -0.25+z	O1	0.5-x, y, 0.5-z	170.435
	O1	0.25-y, -0.25+x, -0.25+z	O1	0.5-x, 0.5-y, z	170.435
	O1	0.25-y, -0.25+x, -0.25+z	O1	x, y, z	174.475
	O1	0.25-y, -0.25+x, -0.25+z	O1	0.25-x, 0.25-y, 0.25-z	5.525
	O1	-0.25+y, 0.25-x, -0.25+z	O1	-0.25+x, -0.25+z, 0.25-y	9.565
	O1	-0.25+y, 0.25-x, -0.25+z	O1	x, 0.5-y, 0.5-z	170.435
	O1	-0.25+y, 0.25-x, -0.25+z	O1	0.5-x, y, 0.5-z	180.000
	O1	-0.25+y, 0.25-x, -0.25+z	O1	0.5-x, 0.5-y, z	170.435
O1	O1	0.5-x, 0.5-y, z	O1	0.5-x, y, 0.5-z	60.000
	O1	0.5-x, 0.5-y, z	O1	x, 0.5-y, 0.5-z	60.000
	O1	0.5-x, 0.5-y, z	Li1	0.5-x, 0.5-y, z	139.211
	O1	x, 0.5-y, 0.5-z	Li1	0.25+y, 0.25-x, 0.25+z	85.217
	O1	x, 0.5-y, 0.5-z	Li1	x, y, z	35.264

## Full Paper

Atom1	Atom2	Symmetry Op.1	Atom3	Symmetry Op.2	Angle213
	Li1	0.5-x, 0.5-y, z	Li1	0.25-y, 0.25+x, 0.25+z	14.385
	Li1	0.5-x, 0.5-y, z	Li1	0.25+y, 0.25-x, 0.25+z	114.385
	Li1	0.5-x, 0.5-y, z	Li1	x, y, z	103.946
	Li1	0.25-y, 0.25+x, 0.25+z	Li1	0.25+y, 0.25-x, 0.25+z	114.385
	Li1	0.25-y, 0.25+x, 0.25+z	Li1	x, y, z	103.946
	Li1	0.25+y, 0.25-x, 0.25+z	Li1	x, y, z	103.946

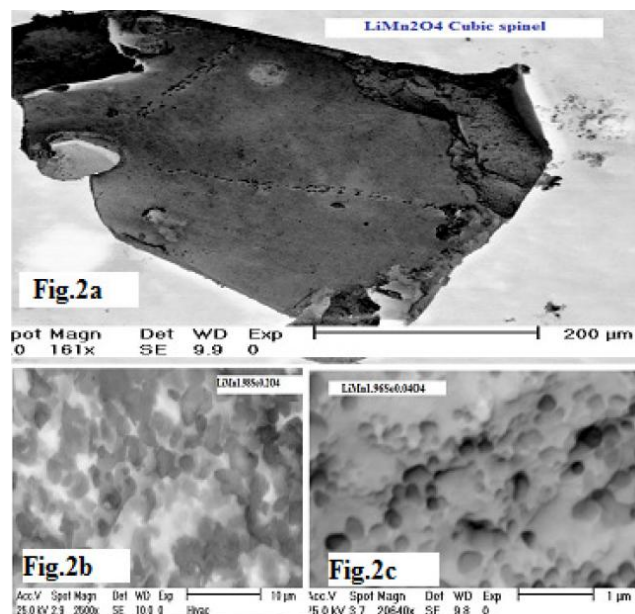


Figure 2 : SE-micrographs captured for pure and Se-substituted spinels. Amplification factor = 200,10 and 1  $\mu$ m. (a): undoped LiMn<sub>2</sub>O<sub>4</sub>; (b): doped with x = 0.02 mole; (c): doped with x = 0.04 mole.

see Figure 4.

Accordingly the enhancement of cycleability/first 10<sup>th</sup> cycles as clear in Figure 4, specially for the sample with optimal doping content x = 0.04 mole is due to Se (IV) resists redox reactions on its immersed electrolyte and stabilize spinel crystal structure by reinforcing lattice stability towards Jahn-Teller distortion inside MnSeO<sub>6</sub>-poly-octahedrons.

It is well known that the two pairs of the oxidation and reduction peaks of LiMn<sub>2</sub>O<sub>4</sub> spinel were located around 4.21 and 4.06 V, corresponding to the two-stage reversible intercalation/deintercalation processes of lithium<sup>[14]</sup>. The results obtained in this study are consistent with those reported previously<sup>[18,30]</sup>. Who is indicating that the oxidation of Mn<sup>3+</sup> to Mn<sup>4+</sup> contributes to the oxidation peaks in the investigated voltage range for the LiMn<sub>2</sub>O<sub>4</sub> and so it is reasonable to assume that only Mn<sup>3+</sup> in both substituted spinels causes the oxidation and reduction peaks<sup>[20]</sup> and that the amount of Mn<sup>3+</sup>

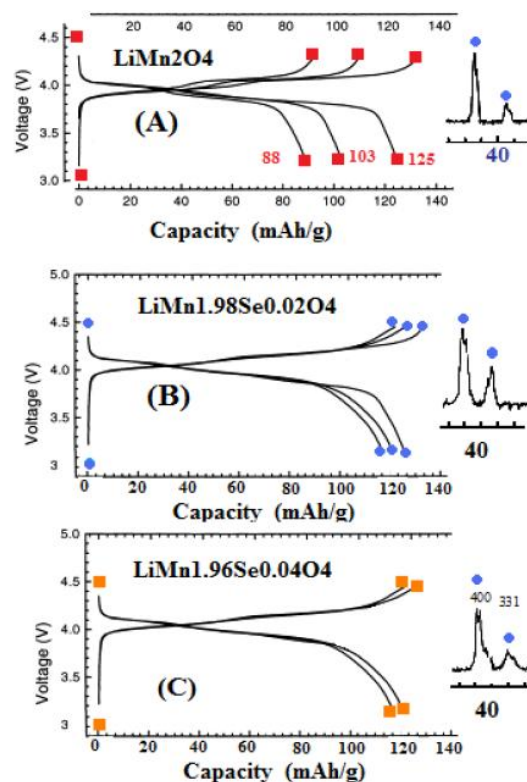


Figure 3<sub>A,C</sub> : First,10<sup>th</sup> and 20<sup>th</sup> cycles of charge and discharge curves of type 2016 coin cells at C/20 rate. Cell—Li-0.5 M LiPF<sub>6</sub> in (1:1 wt.% EC+DEC)—LiMn<sub>2-x</sub>Se<sub>x</sub>O<sub>4</sub>(where x = 0.0,0.02 and 0.04 mole).

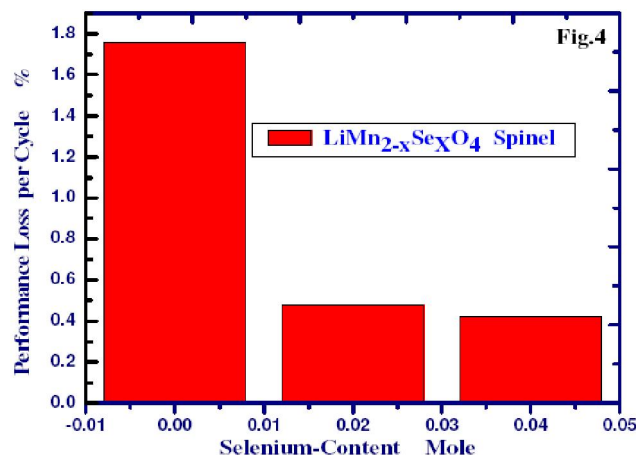


Figure 4 : Performance loss per cycle after first ten cycles versus Se-IV-Doping content.

is decreased by doping, thereby resulting in a decrease in the observed charge capacity.

## CONCLUSIONS

The conclusive remarks can be briefed as follow:

- 1- capacity retentions (performance loss with cycleability) were promoted as Se-doping increases recording maximum for  $x = 0.04$  mole (0.42 % loss per cycle) and 0.48 % loss per cycle is for  $\text{LiMn}_{1.95}\text{Se}_{0.02}\text{O}_4$  and finally minimum one for the undoped parent  $\text{LiMn}_2\text{O}_4$  which equal to 1.76 %.
- 2- charging cathodic capacities recorded were found to be 125, 123, 119  $\text{mA h g}^{-1}$  respectively for pure and Se-substituted spinels with  $x = 0.0, 0.02$  and  $0.04$  mole respectively.

Accordingly the enhancement of recycleability of Se-doped samples specially that with optimal doping content  $x = 0.04$  mole is due to Se (IV) resists redox reactions on its immersed electrolyte and stabilize spinel crystal structure by reinforcing lattice stability towards Jahn-Teller distortion inside  $\text{MnSeO}_6$ -poly-octahedrons.

## REFERENCES

- [1] T.Nagaura, K.Tazawa; Prog.Batteries Solar Cells, **9**, 20 (1990).
- [2] K.Ozawa; Solid State Ionics, **69**, 212 (1994).
- [3] W.Ebner, D.Fouchard, L.Xie; Solid State Ionics, **69**, 238 (1994).
- [4] J.R.Dahn, U.Von Sacken, M.R.Jukow, H.Al-Janaby; J.Electrochem.Soc., **138**, 2207 (1991).
- [5] C.Delmas, I.Saadoune, A.Rougier; J.Power Sources, **43-44**, 595 (1993).
- [6] R.J.Gummow, M.M.Thackeray; J.Electrochem. Soc., **140**, 3365 (1993).
- [7] J.M.Tarascon, W.R.Mckinnon, F.Coowar, T.N.Boowner, G.Amatucci, D.Guyomard; J.Electrochem.Soc., **141**, 1421 (1994).
- [8] D.Guyomard, J.M.Tarascon; Solid State Ionics, **69**, 22 (1997).
- [9] X.Qiu, X.Sun, W.Shen, N.Chen; Solid State Ionics, **93**, 335 (1997).
- [10] Y.K.Sun; Solid State Ionics, **100**, 115 (1997).
- [11] J.M.Tarascon, E.Wang, F.K.Shokoohi, W.R.Mckinnon, S.Colson; J.Electrochem.Soc., **138**, 2589 (1991).
- [12] T.Ohzuoku, M.Kitagawa, T.Hirai; J.Electrochem. Soc., **137**, 769 (1990).
- [13] R.Bittihin, R.Herr, D.Hoge; J.Power Sources, **43-44**, 223 (1993).
- [14] Y.Toyoguchi; Eur.Pat.Appl., **0390**, 185 (1990).
- [15] S.Bach, M.Henry, N.Buffer, J.Livage; J.Solid State Chem., **88**, 325 (1990).
- [16] T.Tsumura, A.Shimizu, M.Inagaki; J.Mater.Chem., **3**, 995 (1993).
- [17] P.Barboux, J.M.Tarascon, F.K.Shokoohi; J.Solid State Chem., **94**, 185 (1991).
- [18] W.Liu, G.Farrington, F.Chaput, B.Dunn; J.Electrochem.Soc., **143**, 879 (1996).
- [19] G.X.Wang, H.K.Liu, S.X.Dou; Solid State Ionics, **120(1-4)**, 95-101 (1999).
- [20] L.Guohua, T.Uchida, M.Wakihara; J.Electrochem. Soc., **143**, 178 (1996).
- [21] A.R.West; In Basic Solid State Chemistry; Wiley, New York, 57 (1991).
- [22] R.Koksang, J.Barker, H.Shi, M.Y.Sa; Solid State Ionics, **84**, 1-21 (1996).
- [23] M.M.Thackeray, W.I.F.David, J.B.Goodenough; Mater.Res.Bull., **17**, 785 (1982).
- [24] M.M.Thackeray; J.Electrochem.Soc., **142**, 2558-2563 (1995).
- [25] R.J.Gummow, A.de kock, M.M.Thackeray; Solid State Ionics, **69**, 59 (1994).
- [26] C.Xu, Y.Tain, Y.C.Zhai, L.Y.Liu; Materials Chemistry and Physics, **98**, 532-538 (2006).
- [27] E.Wolska, M.Tovar, B.Andrzejewski, W.Nowicki, P.Pisora, M.Knapp; Solid State Science, **8**, 31-36 (2006).
- [28] C.H.Lu, S.W.Lin; Journal of Power Sources, **93**, 14-19 (2001).
- [29] H.J.Bang, V.S.Donepudi, J.Prakash; Electrochimica Acta, **48(4)**, 443-451 (2002).
- [30] J.M.Tarascon, D.Guyomard; J.Electrochem.Soc., **138**, 2864 (1991).